Synthesis, evaluation and molecular modeling of cyclic tetrapeptide histone deacetylase inhibitors as anticancer agents

Dawei Huang,[a] Xiaohui Li,[a]* Lei Sun,[a] Zhilong Xiu[a] and Norikazu Nishino[b]

Histone deacetylase inhibitors (HDACIs) are a promising class of anticancer agents. To examine whether a slight change in the recognition domain could alter their inhibitory activity, we synthesized a series of *cyclo*(−L-Am7(S2Py)-Aib-L-Phe(*n*-Me)-D-Pro) derivatives and evaluated their HDAC inhibitory and anticancer activities. The peptides exhibited potent HDAC inhibitory activity and inhibited three human cancer cell lines with IC_{50} in the micromolar range. Docking and molecular dynamics simulation were conducted to explore the interaction mechanisms of class I and II HDACs with these inhibitors. It revealed that the zinc ion in the active site coordinated five atoms of HDACs and the sulfur atom of the inhibitor. The metal binding domains of these compounds interacted with HDAC2, and the surface recognition domains of these compounds interacted with HDAC4 through hydrogen bonding. The hydrophobic interactions also provided favorable contributions to stabilize the complexes. The results obtained from this study would be helpful for us to design some novel cyclic tetrapeptides that may act as potent HDACIs. Copyright © 2012 European Peptide Society and John Wiley & Sons, Ltd.

Keywords: histone deacetylase; histone deacetylase inhibitor; anticancer agent; cyclic tetrapeptide; docking; molecular dynamics

Introduction

Acetylation and deacetylation of ε-amino groups of lysine residues in the N-terminal domain of histone catalyzed by histone acetyltransferase and histone deacetylase (HDAC) play a fundamental role in gene expression because acetylation of histone tails cirelates with an open chromatin configuration and transcriptional activation, and deacetylation induces transcriptional repression through chromatin condensation [1]. In general, HDAC activity correlates to transcriptional repression, and abnormal increase in HDAC activity has been associated with the development of some human cancers [2]. HDACs are classified into four different phylogenetic classes according to their cellular localizations, structural and functional differences: class I (HDAC1–3 and HDAC8) is closely related to yeast Rpd3; class II (HDAC4–7, HDAC9 and HDAC10) have domains that are similar to yeast Hda1; class IV (HDAC11) displays properties of both class I and class II HDACs [3,4]. All the aforementioned HDACs are zinc-dependent proteases and are referred to as 'classical' HDACs. There are seven members of class III HDACs in mammals, and these have been identified on the basis of sequence homology with Sir2, a yeast transcription repressor, and require NAD^+ for their deacetylase activities [5]. The crystal structures of human HDACs (HDAC2 [6], HDAC4 [7] and HDAC8 [8]) show that all have a deep narrow pocket, and a zinc ion is positioned near the bottom of the pocket.

Some studies have shown that inhibition of HDACs produces anticancer effects in several tumor cell lines. Normal cells are more resistant to the cell-death-inducing effect of HDAC inhibitors (HDACIs) than cancer cells [9,10]. HDACIs have been developed for anticancer chemotherapy in the recent years. Some natural and synthetic compounds have been reported to act as HDACIs, such as trichostatin A (TSA) [11], vorinostat (suberoylamilide hydroxamic acid) [12] and some cyclic tetrapeptides, such as apicidin [13], FK228 [14–16] and chlamydocin [17] (Figure 1). The zinc-binding site of FK228 is the sulfhydryl group, and FK228 is converted to its active form (RedFK228) by cellular reducing activity. FK228 (Romidepsin international nonproprietary name, trade name Istodax (Gloucester Pharmaceuticals, Cambridge, Mass., USA)) was approved by the U.S. Food and Drug Administration for the treatment of cutaneous T-cell lymphoma, after 5 years in the agency's fast track development program.

Chlamydocin was originally isolated from the fungus *Diheterospora chlamydosporia*. It contains Aib (α-aminoisobutyric acid), L-Phe, D-Pro and L-Aoe (L-amino-8-oxo-9,10-epoxydecanoic acid), which react and inhibit HDACs [18]. Hydrophobicity at the surface recognition domain of HDACIs is crucial for their activities, and the cyclic tetrapeptide framework has a significant structural role in the specific hydrophobic interaction with the surface of HDACs. The role and the appropriate position of the aromatic ring of L-Phe in the chlamydocin macrocycle have been investigated, and the data indicated that L-Phe was important for interacting with the surface binding region of HDACs [19].

In order to find some specific inhibitors, we designed and synthesized several novel cyclic tetrapeptides with methyl L-Phe in their macrocyclic frameworks. The importance of L-Phe has stimulated our interest to study whether slight change to the

* Correspondence to: Xiaohui Li, School of Life Science and Biotechnology, Dalian University of Technology, Dalian 116024, China. E-mail: lxhxh@dlut.edu.cn

a School of Life Science and Biotechnology, Dalian University of Technology, Dalian 116024, China

b Graduate School of Life Science and Systems Engineering, Kyushu Institute of Technology, Kitakyushu 808-0196, Japan
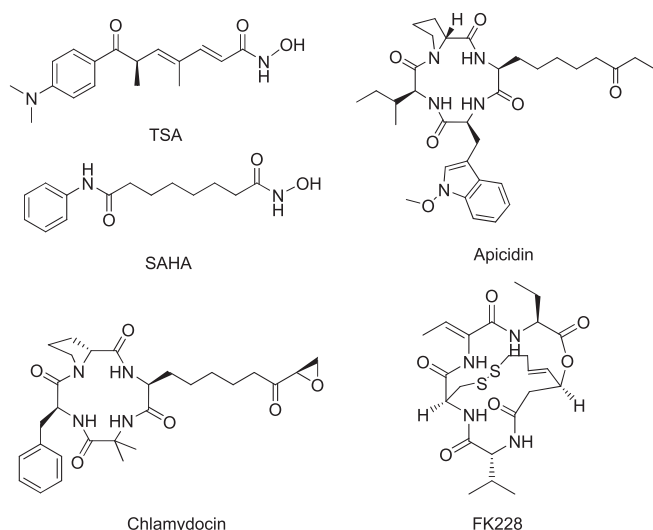
Figure 1. Structures of some HDACIs.

aromatic ring of L-Phe could alter the inhibitory activity of inhibitor against HDAC. The metal binding domain of these compounds was the sulfhydryl group that was protected as disulfide hybrid (Figure 2), but it could be reduced to sulfhydryl group by intracellular L-glutathione.

Cyclic tetrapeptides are the most structurally complex HDACIs, but the interaction between these inhibitors and HDACs is only partly known. Studies analyzing the binding between HDAC-like protein (HDLP), which shares 35% sequence identity with human HDAC1, and the cyclic tetrapeptides, FR235222 and azumamide E, have been published [20,21], but the detail of interaction between human HDACs and cyclic tetrapeptide type HDACIs is still not available.

Conformational analysis of HDACs with their inhibitors is very helpful for elucidating the structure–activity relationship behavior between enzyme and inhibitor, and for designing new drug candidates. Molecular dynamics (MD) simulation is a very useful technique for exploring the structure and the dynamic behavior of molecules of biochemical interest. To explore the mechanism by which HDACs interact with these sulfur-containing cyclic tetrapeptide inhibitors and to compare the different modes by which these inhibitors bind to class I and II HDACs, docking and MD simulations were conducted for HDAC2, which shares 82% sequence identity with HDAC1, and HDAC4 with these inhibitors.
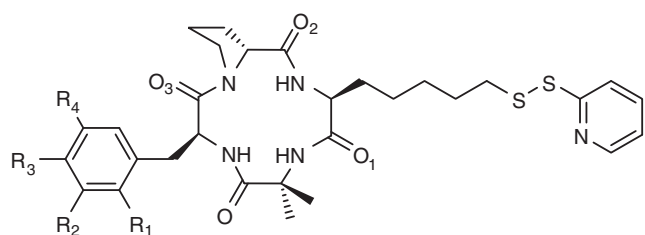
1. R₁=H, R₂=H, R₃=H, R₄=H *cyclo*(-L-Am7(S2Py)-Aib-L-Phe-D-Pro-)
2. R₁=CH₃, R₂=H, R₃=H, R₄=H *cyclo*(-L-Am7(S2Py)-Aib-L-Phe(2-Me)-D-Pro-)
3. R₁=H, R₂=H, R₃=CH₃, R₄=H *cyclo*(-L-Am7(S2Py)-Aib-L-Phe(4-Me)-D-Pro-)
4. R₁=H, R₂=CH₃, R₃=H, R₄=CH₃ *cyclo*(-L-Am7(S2Py)-Aib-L-Phe(3,5-2Me)-D-Pro-)

Figure 2. Structures of synthesized cyclic tetrapeptides.

Experiments and Computational Methodology

Synthesis

Synthesis of Boc-L-α-amino-7-bromoalkanoic (Boc-L-Ab7-OH) and Boc-L-methylphenylalanines (Boc-L-Phe(n-Me)-OH)

Boc-L-Ab7-OH and Boc-L-Phe(*n*-Me)-OH were synthesized according to the procedure reported in [22], and the overall yield was 35%–40%.

Synthesis of cyclo(−L-Am7(S2Py)-Aib-L-Phe-D-Pro)

This compound was synthesized according to conventional solution phase method. H-D-Pro-OBzl (2 mmol), Boc-L-Phe-OH (2.2 mmol), HOBt·H₂O (2 mmol) and DCC (2 mmol) were added in DMF (4 ml), and the solution was stirred overnight. After evaporation of DMF, the residue was extracted and purified using silica gel chromatography (CHCl₃ : MeOH = 99 : 1) to yield Boc-L-Phe-D-Pro-OBzl (1.91 mmol). Boc group was then removed using 4 N HCl/dioxane (6 ml) and then the N-terminus free dipeptide (1.91 mmol), Boc-Aib-OH (2.2 mmol), HBTU (2.2 mmol) and HOBt·H₂O (2 mmol) were added in DMF (4 ml) and stirred overnight. Boc-Aib-L-Phe-D-Pro-OBzl (1.18 mmol) was obtained in the same manner as described earlier. The N-terminus of the tripeptide was deprotected using 4 N HCl/dioxane (3.6 ml), and the N-terminus free tripeptide (1.18 mmol) was coupled with Boc-L-Ab7-OH (1.3 mmol) using HOBt·H₂O (1.3 mmol) and DCC (1.3 mmol) to yield tetrapeptide. Boc-L-Ab7-Aib-L-Phe-D-Pro-OBzl (0.84 mmol) was obtained after purification using silica gel chromatography (CHCl₃ : MeOH = 99 : 1). After the C-terminal benzyl protection was removed using catalytic hydrogenation, the N-terminal Boc group was removed using treatment with TFA (2.5 ml). Cyclization reaction was carried out in DMF (840 ml), the linear tetrapeptide (0.84 mmol), HATU (1.3 mmol) and DIEA (2.1 mmol) was added, and the solution was stirred for 3 h. The yield of cyclic tetrapeptide was 61% (0.51 mmol) after purification using silica gel chromatography (CHCl₃ : MeOH = 99 : 1). The cyclic tetrapeptide (0.51 mmol) containing L-Ab7 was reacted with potassium thioacetate (0.75 mmol) for 5 h to convert the bromide to thioacetate ester, *cyclo*(−L-Am7(SAc)-Aib-L-Phe-D-Pro) (0.47 mmol). To a solution of *cyclo*(−L-Am7(SAc)-Aib-L-Phe-D-Pro) in DMF (2 ml) under argon atmosphere, the 2,2′-dipyridyl disulfide (0.9 mmol) and 40% NH₂CH₃/MeOH (2.5 mmol) were added and stirred for 5 h. The target compound, *cyclo*(−L-Am7(S2Py)-Aib-L-Phe-D-Pro) was obtained after purification using silica gel chromatography (CHCl₃ : MeOH = 99 : 1). Its overall yield was 7.4%. (High resolution) HR-FAB-MS [M + H]⁺ 598.2478 for C₃₀H₃₉O₄N₅S₂ (calculated 598.2522); ¹H NMR (CDCl₃, 400 MHz, δ, ppm) 1.27 (2H, m), 1.34 (3H, s), 1.42 (2H, m), 1.61 (2H, m), 1.71 (2H, m), 1.77 (3H, s), 1.88 (2H, m), 2.17 (1H, m), 2.25 (1H, m), 2.78 (1H, m), 2.96 (1H, m), 3.23 (2H, m), 4.19 (2H, m), 4.66 (2H, d, *J* = 6.2 Hz), 5.17 (1H, m), 6.06 (1H, s), 7.11 (1H, m), 7.21 (1H, d, *J* = 4.1 Hz), 7.25 (5H, m), 7.51 (1H, d, *J* = 9.9 Hz), 7.66 (1H, m), 7.73 (1H, d, *J* = 8.0 Hz), 8.47(1H, d, *J* = 5.6 Hz); ¹³C NMR (CDCl₃, 400 MHz, δ, ppm) 23.57, 24.75, 25.02, 25.09, 26.47, 28.06, 28.61, 28.83, 35.82, 38.66, 46.99, 53.43, 54.30, 57.78, 58.81, 119.62, 120.55, 126.72, 128.62, 128.62, 129.04, 129.04, 137.01, 137.04, 149.60, 160.54, 171.85, 172.84, 174.33, 175.63.

Synthesis of cyclo(−L-Am7(S2Py)-Aib-L-Phe(2-Me)-D-Pro)

This compound was synthesized according to *cyclo*(−L-Am7(S2Py)-Aib-L-Phe-D-Pro) using Boc-L-Phe(2-Me)-OH instead of Boc-L-Phe-OH. Its overall yield was 8.2%. HR-FAB-MS [M + H]⁺ 612.2722 for

$C_{31}H_{41}O_4N_5S_2$ (calculated 612.2679); ^{1}H NMR (CDCl$_3$, 400 MHz, δ, ppm) 1.08 (1H, m), 1.32 (1H, m), 1.34 (3H, s), 1.37 (3H, m), 1.60 (1H, m), 1.66 (3H, s), 1.70 (2H, m), 1.77 (2H, s), 1.93 (2H, m), 2.31 (1H, m), 2.39 (3H, s), 2.78 (1H, t), 2.96 (1H, m), 3.23 (1H, m), 3.44 (1H, m), 3.84 (1H, m), 4.18 (1H, m), 4.68 (1H, m), 5.19 (1H, m), 6.01 (1H, s), 7.11 (1H, m), 7.13 (1H, m), 7.26 (4H, s), 7.52 (1H, d, $J = 10.1$ Hz), 7.65 (1H, m), 7.71 (1H, m), 8.46 (1H, d, $J = 4.3$ Hz); ^{13}C NMR (CDCl$_3$, 400 MHz, δ, ppm) 19.72, 23.70, 24.86, 25.08, 26.46, 28.17, 28.72, 29.35, 33.02, 34.08, 38.72, 46.97, 52.35, 54.44, 57.87, 58.87, 119.69, 120.20, 126.20, 126.91, 129.43, 130.55, 135.35, 136.60, 137.15, 149.71, 160.62, 171.97, 173.03, 174.53, 175.80.

Synthesis of cyclo(−L-Am7(S2Py)-Aib-L-Phe(4-Me)-D-Pro)

This compound was synthesized according to *cyclo*(−L-Am7(S2Py)-Aib-L-Phe-D-Pro) using Boc-L-Phe(4-Me)-OH instead of Boc-L-Phe-OH. Its overall yield was 9.5%. HR-FAB-MS $[M + H]^+$ 612.2680 for $C_{31}H_{41}O_4N_5S_2$ (calculated 612.2679); ^{1}H NMR (CDCl$_3$, 400 MHz, δ, ppm) 0.86 (1H, m), 1.28 (3H, m),1.34 (3H, s), 1.42 (2H, m), 1.70 (3H, m), 1.78 (3H, s), 1.80 (2H, m), 2.17 (1H, m), 2.26 (3H, s), 2.33 (1H, m), 2.78 (1H, t), 2.88 (1H, m), 3.17 (1H, m), 3.27 (2H, m), 4.17 (1H, m), 4.66 (1H, d, $J = 6.1$ Hz), 5.15 (1H, m), 5.96 (1H, s), 6.84 (3H, s), 7.09 (2H, m), 7.27 (1H, s), 7.49 (1H, d, $J = 10.2$ Hz), 7.66 (1H, t), 7.72 (1H, d, $J = 8.2$ Hz), 8.46 (1H, d, $J = 4.1$ Hz); ^{13}C NMR (CDCl$_3$, 400 MHz, δ, ppm) 21.05, 23.57, 24.76, 25.04, 25.1, 26.53, 28.08, 28.62, 28.79, 35.37, 38.67, 47.00, 53.49, 54.26, 57.78, 58.84, 119.61, 120.54, 128.88, 128.88, 129.30, 129.30, 133.89, 136.21, 136.99, 149.62, 160.56, 171.85,172.90, 174.29, 175.63.

Synthesis of cyclo(−L-Am7(S2Py)-Aib-L-Phe(3,5-2Me)-D-Pro)

This compound was synthesized according to *cyclo*(−L-Am7(S2Py)-Aib-L-Phe-D-Pro) using Boc-L-Phe(3,5-Me)-OH instead of Boc-L-Phe-OH. Its overall yield was 8.7%. HR-FAB-MS: $[M + H]^+$ 626.2814 for $C_{32}H_{43}O_4N_5S_2$ (calculated 626.2835); ^{1}H NMR (CDCl$_3$, 400 MHz, δ, ppm) 0.80 (1H, m), 1.28 (2H, m), 1.34 (3H, s), 1.42 (2H, m), 1.60 (1H, m), 1.69 (3H, m), 1.77 (3H, s), 2.17 (1H, m), 2.30 (6H, s), 2.33 (1H, m), 2.78 (2H, t), 2.90 (1H, m), 3.22 (2H, m), 3.87 (1H, m), 4.17 (1H, m), 4.65 (1H, s), 5.14 (1H, m), 5.92 (1H, s), 6.84 (3H, s), 7.09 (1H, m), 7.27 (2H, s), 7.49 (1H, d, $J = 10.4$ Hz), 7.66 (1H, t), 7.72 (1H, d, $J = 8.2$ Hz), 8.46 (1H, d, $J = 4.4$ Hz); ^{13}C NMR (CDCl$_3$, 400 MHz, δ, ppm) 21.26, 21.26, 23.57, 24.76, 25.05, 25.09, 26.53, 28.07, 28.62, 28.79, 35.64, 38.68, 47.01, 53.40, 54.25, 57.79, 58.84, 119.62,120.53, 126.82, 128.82, 128.33, 136.9, 136.97, 137.99, 137.99, 149.61, 160.57, 171.84, 172.91, 174.29, 175.57.

Conformation Studies using CD and NMR

The CD spectra of all compounds were carried out in methanol with peptide concentration of 0.1 mM. The solution conformation of compound **2** was studied using ^{1}H NMR in CDCl$_3$. Complete assignments were made using COSY and NOESY spectra. The $J_{NH-HC\alpha}$ values were obtained from NMR charts. The structure of compound **2** with minimum energy was generated using molecular operating environment (MOE) program.

HDAC Inhibition Assay

The disulfide bond of each compound was reduced using dithiothreitol (DTT) to give a sulfhydryl group that acts as metal binding domain before the assay. Compound **1** (598 mg) and DTT (385 mg) were added to a mixture of water (10 ml) and acetonitrile (3 ml), and the mixture was left at room temperature for 24 h. The acetonitrile was removed via evaporation. The mixture

was then purified using preparative HPLC, and the yield of reduced compound **1** was 25.7%. Reduced compounds **2**, **3** and **4** were obtained using the same method, and their yields were 27.8%, 26.1% and 25.2%, respectively.

The HDAC inhibitory activities of all compounds were assayed with the HDAC Fluorometric/Drug Discovery Assay Kits (AK511 and AK500; BioMol (Farmingdale, NY 11735, USA)) according to the manufacturer's instructions. Each compound was assayed in triplicate, and the assay was repeated three times. The IC$_{50}$ values were calculated using SPSS 17.0 (SPSS Inc., Chicago, IL, USA).

Inhibition Against Cancer Cell Growth

Growth inhibition was determined using the MTT 3-(4,5)-dimethylthiahiazo (-z-y1)-3,5-di-phenytetrazoliumromide assay. Human breast cancer cells MCF-7 (human breast cancer), HeLa (human cervix cancer) and 7721 (human liver cancer) cells were all cultured in RPMI 1640 medium supplemented with 10% fetal bovine serum. Cell cultures were incubated in a humidified atmosphere of 5% CO_2 in air. Cells were diluted to $5–9 \times 10^4$ cells/ml with the corresponding medium and were plated in 96-well microplate. A serial dilution of the compound to be evaluated was added, and the plate was incubated for 48 h. After incubation, 200 μl MTT (0.5 mg/ml) reagent diluted in serum-free medium (0.5 mg/ml) was added to each well, and the cells were incubated for an additional 4 h followed by addition of 200 μl DMSO to dissolve the dark blue crystal (formazan). The optical density of the plate was measured at 570 nm with a microplate spectrophotometer. All experiments were performed in triplicate and repeated three times. The IC$_{50}$ values were calculated using SPSS 17.0 (SPSS Inc.).

Docking Studies

Docking studies were conducted with AutoDock4.0 (The Scripps Research Institute (TSRI), La Jolla, California, USA) program [23,24] using a Lamarckian genetic algorithm. AutoDock docking protocol and scoring function have been successfully applied in the interpretation of the inhibitory activity of several HDACIs [21,25]. Initial structure of HDAC2 and HDAC4 were modeled from the atom coordinates of the X-ray crystal structure (protein data bank (PDB) code: 3MAX and 2VQJ, respectively). The active site of HDACs was covered using a grid box size of $70 \times 70 \times 70$ points with a spacing of 0.375 Å between the grid points. For the cyclic tetrapeptides, all single bonds except the amide bonds and cyclic bonds were treated as active torsional bonds. For each inhibitor, 200 independent dockings, i.e. 200 runs, were performed using genetic algorithm searches. A maximum number of 250 000 000 energy evaluations and a maximum number of 10 000 generations were implemented during each genetic algorithm run. The default non-bonded zinc parameters in AutoDock4.0 [23] were employed. The LigPlot program (Wallace AC, Laskowski RA and Thornton JM, London, UK) [26] was also employed to analyze the docking results focusing on hydrogen bonds and hydrophobic contacts.

MD Simulation

All the molecular mechanics and dynamics calculations were carried out with the Amber9 [27] package. The standard amber ff99 force field [28] was used as the parameters for the protein and water atoms, and the general amber force field [29] and austin model 1-bond charge correction (AM1-BCC) charges [30] were used for the ligands. Zinc was modeled using the Stote non-bonded

model ($q = +2e^-$, $r = 1.7$ Å, $\varepsilon = 0.67$ kcal/mol) [31]. Each initial structure for the simulation was prepared from the docked conformations of HDAC2-compound **3** and HDAC4-compound **3** complexes. The local hydrogen bonding network around the histidine residues was checked. His183 of HDAC2 and His198 of HDAC4 were assigned as HIE (histidine with hydrogen on its epsilon nitrogen), and other histidine residues as HID (histidine with hydrogen on its delta nitrogen). The force field parameters of compound **3** were prepared using Antechamber module [32] of Amber9 package. Hydrogen atoms were added to the crystallographic protein with the Amber9 Leap module. Sodium counterions were added to neutralize the system. The system was then solvated with an octahedral box of TIP3P water molecules [33]. The minimum distance from the surface of the protein to the faces of the box was 10 Å. The particle mesh Ewald method [34] was used to treat long-range electrostatic interactions. The cutoff distance for the long-range electrostatic and the van der Waals energy terms were set at 12.0 Å. All covalent bonds to hydrogen atoms were constrained using the SHAKE algorithm [35].

Energy minimization was achieved in three steps. In the first step, movement was allowed only for the water molecules and ions. In the second step, the inhibitor and the enzyme residues were all allowed to move and the water molecules, together with ions, were constrained. In the final step, all atoms were permitted to move freely. In each step, energy minimization was executed by the steepest descent method for the first 5000 steps and the conjugated gradient method for the subsequent 2500 steps.

Periodic boundary conditions were used. The time steps were 2 fs during the production dynamics. The temperature was maintained by rescaling the velocities using the Berendsen weak-coupling algorithm [36], with a time constant of 2 ps for the heat bath. After the system was heated to 300 K from the initial temperature of 0 K using the constant number, volume and temperature (NVT) ensemble in 120 ps, molecular dynamics were performed at a constant temperature of 300 K. After a 50 ps position-restrained dynamics, each simulation proceeded for 2 ns under periodic boundary conditions with constant number, pressure and temperature (NPT) ensemble at 101325 pascal and at 300 K. The convergence of energies, temperatures, pressures of the systems and the atomic root mean square deviations (RMSD) of the enzyme and the inhibitor, were used to verify the stability of the systems. Trajectories were analyzed using the Ptraj modules [37]. In the present MD simulations, the overall structure of all complexes appeared to be equilibrated after 1.5 ns. Hence, atom coordinates were collected at an interval of 5 ps for the last 500 ps to analyze the structure in detail. The series of snapshots between 1.5 and 2 ns of the equilibrium phase was used for further analysis.

Results and Discussion

Chemistry

In order to synthesize potent HDACIs that had the similar cyclic framework to chlamydocin, we prepared the non-natural amino acids Boc-L-Ab7-OH and Boc-L-Phe(n-Me)-OH. Target cyclic tetrapeptides were synthesized according to conventional solution phase method. All the compounds shown were confirmed using HR-FAB-MS, ^{1}H NMR and ^{13}C NMR.

Conformation Studies

The CD spectrum of each synthesized compound was similar at 190–260 nm (Figure 3). These compounds had two negative
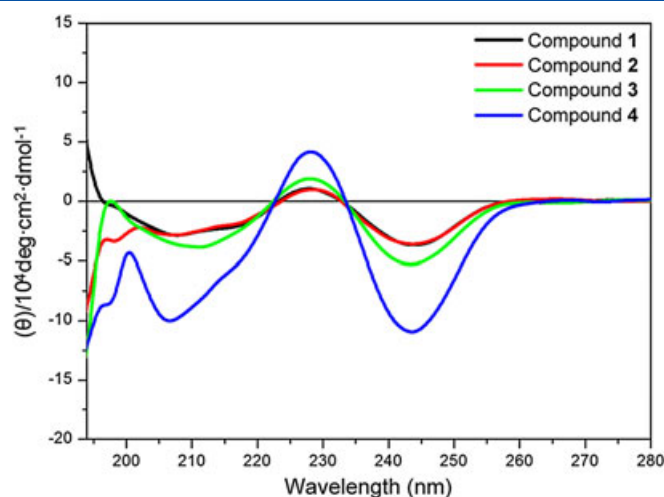
Figure 3. CD spectra of compounds **1–4**.

ellipticities at 210 and 245 nm, and a weak positive ellipticity at 230 nm. Compound **4** had a sharp ellipticity because of containing two methyl groups (L-Phe(3,5-Me)). These similarities on CD spectra suggested that the peptide backbone of these compounds had similar structures. This explained the fact that the change of methyl positions in L-Phe(n-Me) could not affect their conformations. The energy-minimized structure of compound **2** was shown in Figure 4.

HDAC Inhibition Assay

All compounds were tested for their HDAC inhibitory activity in vitro, and TSA was used as positive control. The dose–response curves of all synthesized compounds are shown in Figure 5, and the IC$_{50}$ values of all compounds against HDAC1 and HDACs are presented in Table 1. All compounds showed potent HDAC inhibitory activities that were comparable with the activity of TSA. The similar HDAC inhibition abilities of all compounds revealed that introduction of methyl groups on the aromatic ring of L-Phe in this series of HDACIs did not interfere with the contacts between inhibitors and enzymes.

Inhibition Against Cancer Cell Growth

Compounds **1–4** were tested for in vitro antiproliferative activity against MCF-7, Hela and 7721 cell lines using MTT assays. As the dose–response curves of all compounds (Figure 6) and the
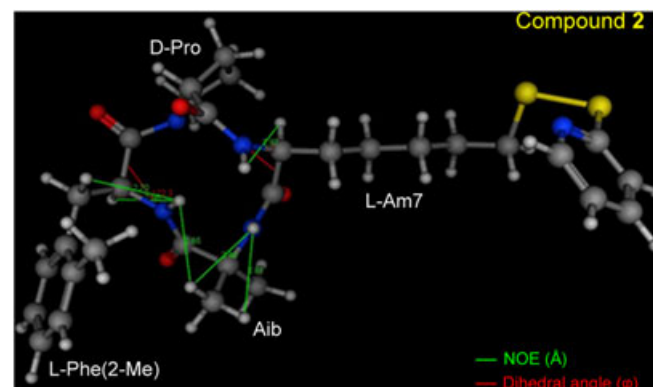
Figure 4. The energy-minimized structure of compound **2** using NMR calculation.
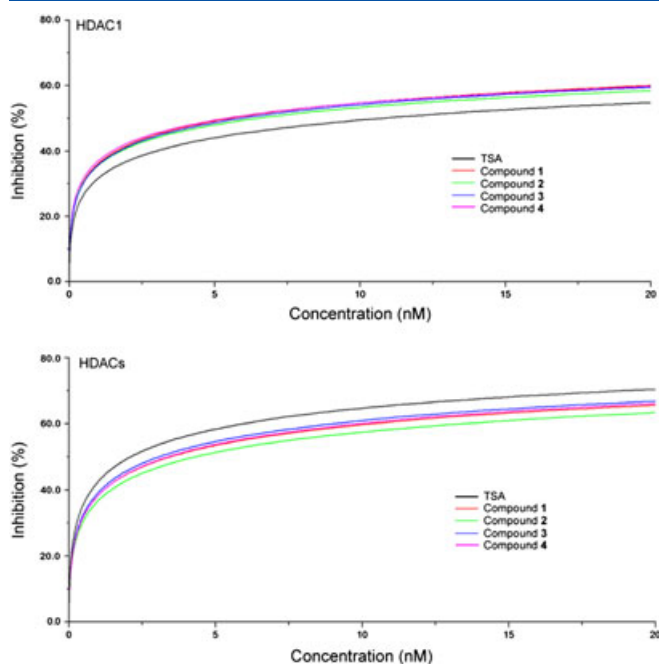
Figure 5. Dose–response curves of all synthesized compounds for inhibitory activity against HDAC1 and HDACs.

IC$_{50}$ values (Table 1) showed, all compounds inhibited the proliferation of these cancer cells at low concentration, thus exhibiting good anticancer activity. There were no obvious differences in antiproliferative activity among the different compounds, but all seemed to exhibit about 20-fold more selectivity than 7721 in the inhibition of Hela cells.

Docking Studies

The results of docking for compounds **1–4** into HDAC2 and HDAC4 are shown in Figure 7. All compounds bound to the active sites of HDACs with a similar pattern. The aliphatic chain occupied the long and narrow channel, the sulfhydryl group was at the bottom of this channel, and the large cap domain interacted with the external surface of the enzyme. In HDAC2-inhibitor complexes, the aromatic rings of L-Phe were all at the groove formed by Tyr209 and Phe210, and in HDAC4-inhibitor complexes, the aromatic rings interacted with Phe227. The adjacent methylene group caused the aromatic ring to move to the appropriate position, so no difference in binding to HDACs was detected among the compounds, though the introduced methyl groups could enhance the hydrophobicity and steric hindrance of L-Phe.

The distances between sulfur atoms of all compounds and zinc ion in the active site of HDAC2 were 2.5, 2.2, 2.4 and 2.3 Å,

Figure 6. Dose–response curves of all synthesized compounds for antiproliferative activity against cancer cell lines.

respectively, and between sulfur atoms of all compounds and zinc ion in the active site of HDAC4 were 2.7, 2.3, 2.2 and 2.3 Å, respectively.

Binding energy study showed that no real difference in binding energy occurred between the complexes formed by inhibitor and HDAC2 and those formed by inhibitor and HDAC4 (Table 2), and this was in accordance with the fact that these compounds had similar affinities for enzymes. It could be concluded that the introduction of methyl groups on the aromatic ring of L-Phe did not affect the ability of these compounds to bind to HDACs, so the slight changes in hydrophobicity and steric hindrance on the large surface recognition domain of cyclic tetrapeptide HDACIs had little effect on their interactions with the surface binding region of HDACs.

The interactions between all compounds and HDACs from docking results were almost the same, so only one of the compounds, compound **3**, was chosen for further analysis. Hydrogen bonds and hydrophobic contacts between HDACs and compound **3** are shown in Figure 8. In HDAC2–compound **3** complex, the sulfur atom of compound **3** established hydrogen bonds with the OH atom of Tyr308 and the ND1 atom of His183, and in HDAC4–compound **3** complex, the sulfur atom of compound **3** formed hydrogen bond with the NE2 atoms of both His158 and His159. In docked HDLP–cyclic tetrapeptide inhibitor complexes, the hydrogen bonds were formed between the carboxyl group

Table 1. The IC$_{50}$ values of all synthesized compounds against enzymes and cancer cell lines

Compound	Enzymes (nM)		Cell lines (µM)		
	HDAC1	HDACs	MCF-7	Hela	7721
TSA	8.19	1.77	—	—	—
1	4.30	2.85	3.60	0.54	11.51
2	4.90	3.52	3.86	0.51	11.17
3	4.57	2.56	4.12	0.46	12.08
4	4.08	2.81	3.30	0.48	11.76
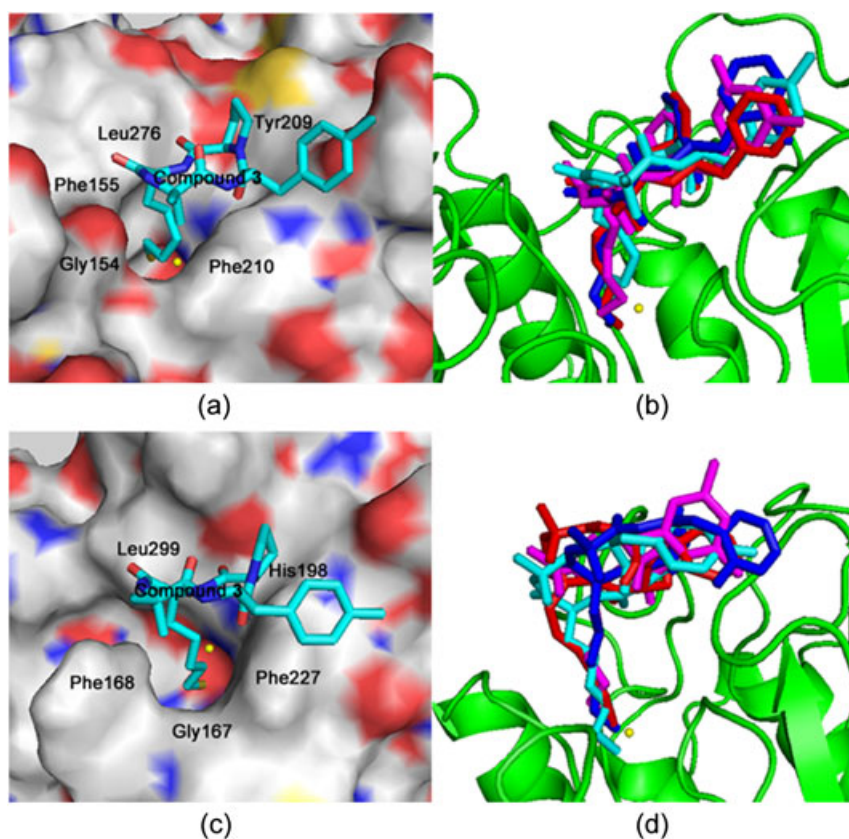
Figure 7. Views of the active site regions of (a) HDAC2–Compound **3**; (b) HDAC2–Compound **1–4**; (c) HDAC4–Compound **3**; (d) HDAC4–Compound **1–4** from docking results.

and hydroxyl group in the metal binding domain of the inhibitors and the corresponding His131, His132, Asp168 and Tyr297 of HDLP [20,21]. It suggested that the hydrogen bonds formed by the metal binding domain were important for the cyclic tetrapeptide HDACIs with powerful inhibitory activity.

Compound **3** also made contact with some other amino acid residues of HDACs, such as Phe155, Glu208, Tyr209, Phe210 and Leu276 of HDAC2, His198, Phe226, Phe227, Pro298 and Leu299 of HDAC4 via hydrophobic interaction. Hydrophobic interaction also occurred between cyclic tetrapeptide HDACIs and HDLP [20,21], and this interaction was also crucial for stabilizing the complexes.

MD Simulations

The MD simulations were performed for the HDAC2–compound **3** and HDAC4–compound **3** complexes. Both of the complexes converged and were stable as indicated by their energetic and structural properties. The potential energies and RMSD remained stable during the last 500 ps of the simulations for the two complexes. The RMSD between C_{α}, C and N atoms of the structures obtained during the trajectories and initial structures are shown in Figure 9.

The root mean squared fluctuation (RMSF) of C_{α}, C and N atoms for these complexes showed that the structures of the two complexes shared different RMSF distribution (Figure 10), but the conformational changes of the amino acid residues in the active site were all very small, especially for those residues at the bottom of the channel (His145, His146, Asp181, His183 and Asp269 of HDAC2, His158, His159, Asp196, His198 and Asp290 of HDAC4) (Figure 11). This indicated that binding modes of compound **3** in the active site of HDAC2 and HDAC4 were similar, and the binding between HDACs and the inhibitor directly caused the rigidity of the channel.

Table 2. Binding energies of all compounds to HDACs from docking

Energy (kcal/mol)	HDAC2				HDAC4			
	1	2	3	4	1	2	3	4
$E_{binding}$	−5.66	−5.86	−5.74	−5.76	−5.75	−5.88	−5.94	−5.85
$E_{intermolecular}$	−7.67	−7.99	−7.79	−7.87	−7.69	−7.65	−7.86	−7.71
$E_{vdW + Hbond + desolv}$	−7.26	−7.44	−7.29	−7.35	−7.33	−7.27	−7.51	−7.39
$E_{electrostatic}$	−0.41	−0.55	−0.50	−0.52	−0.36	−0.38	−0.35	−0.32
$E_{total\ internal}$	−0.89	−0.62	−0.75	−0.72	−0.82	−0.79	−0.88	−0.84
$E_{torsional}$	2.20	2.20	2.20	2.20	2.20	2.20	2.20	2.20
$E_{unbound}$	−0.61	−0.65	−0.61	−0.63	−0.62	−0.66	−0.60	−0.63

Key
- ●—● Ligand bond
- ●—● Non-ligand bond
- ●--●3.1--● Hydrogen bond and its length
- His 53 Non-ligand residues involved in hydrophobic contact(s)
- ● Corresponding atoms involved in hydrophobic contact(s)
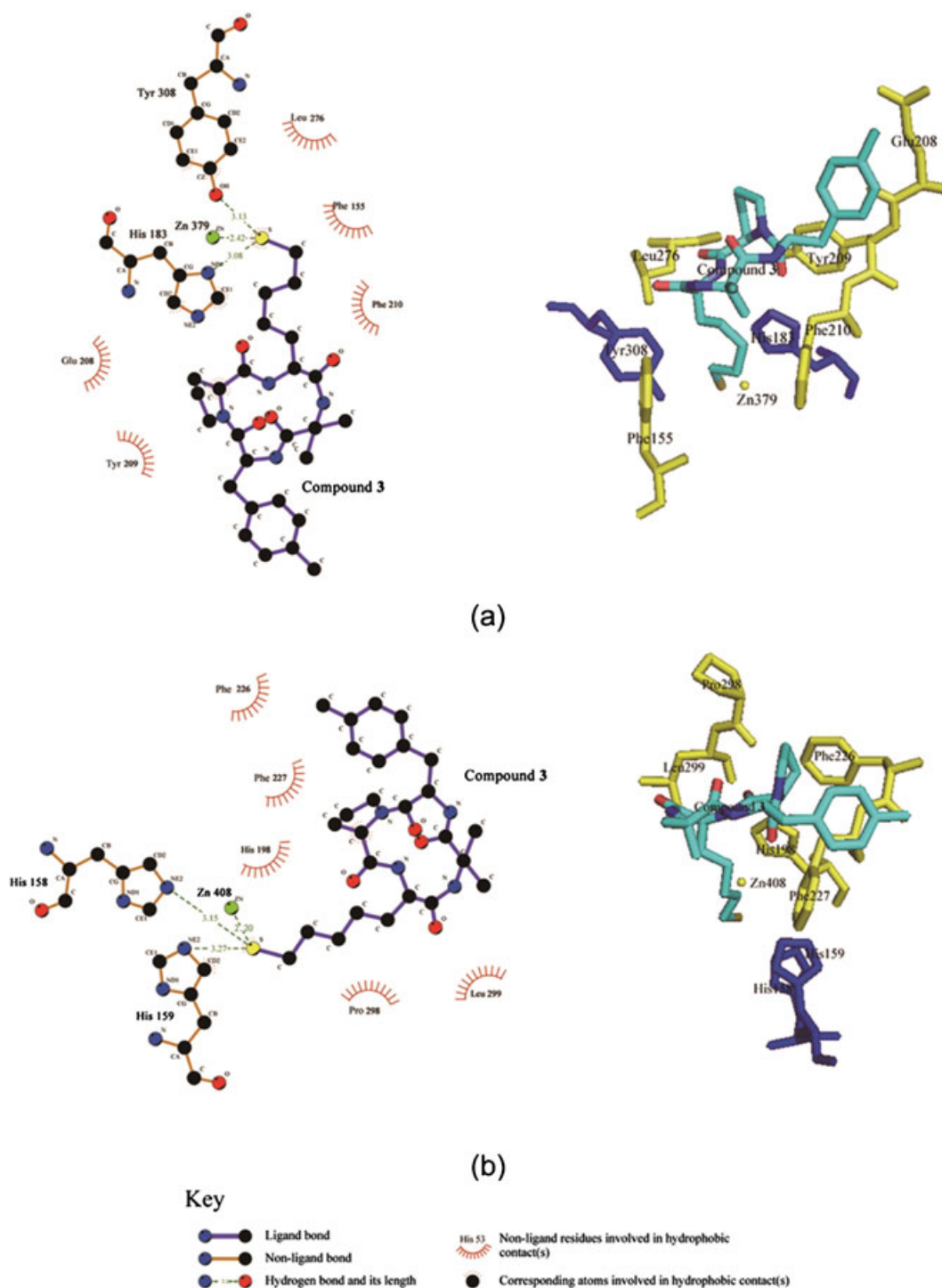
Figure 8. Hydrogen bonds and hydrophobic contacts between (a) HDAC2 and (b) HDAC4 and compound **3**. Blue, amino acids that create hydrogen bonds; yellow, amino acids that form hydrophobic interaction.

In the crystal structure of HDAC–inhibitor complex, the zinc ion that lies at the end of the hydrophobic channel is bound to the carboxylate oxygens of Asp181, Asp269 and the nitrogen atom of His183 of HDAC2 and corresponding Asp169, Asp290, and His198 of HDAC4. The other two coordination sites are occupied by two atoms of the inhibitors [6,7]. The average distances between the zinc ion and the nearby atoms during the last 500 ps in MD simulations are shown in Figure 12, where it can be seen that the zinc atom coordinated with six atoms. In HDAC2–

compound **3** complex, the atoms included all carboxylate oxygens of Asp181 and Asp269, a nitrogen atom of His183 and a sulfur atom of the inhibitor; in HDAC4–compound **3** complex, there were two carboxylate oxygens of Asp196, a carboxylate oxygen of Asp290, nitrogen atoms of His158 and His198 and a sulfur atom of the inhibitor. This showed that all the aspartic acid and histidine residues in the bottom of active site of HDACs could coordinate zinc ion in the MD simulation. The coordination states of zinc ion in both HDAC2–compound **3** and HDAC4–compound
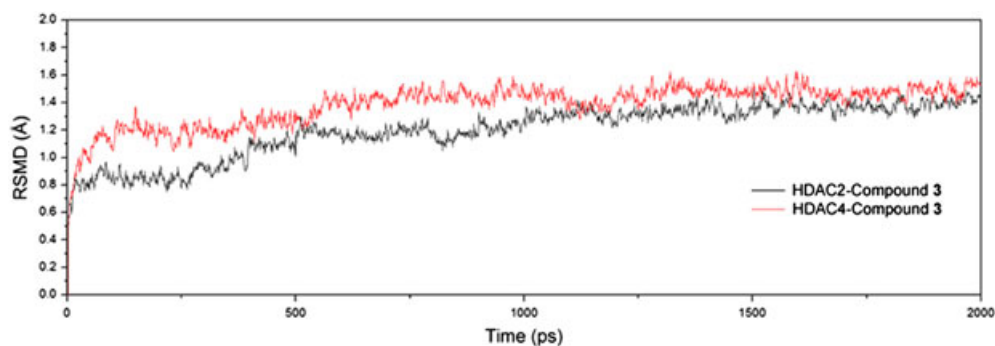
Figure 9. RMSD of C$_\alpha$, C and N atoms of the systems in MD simulations with respect to the starting structure.
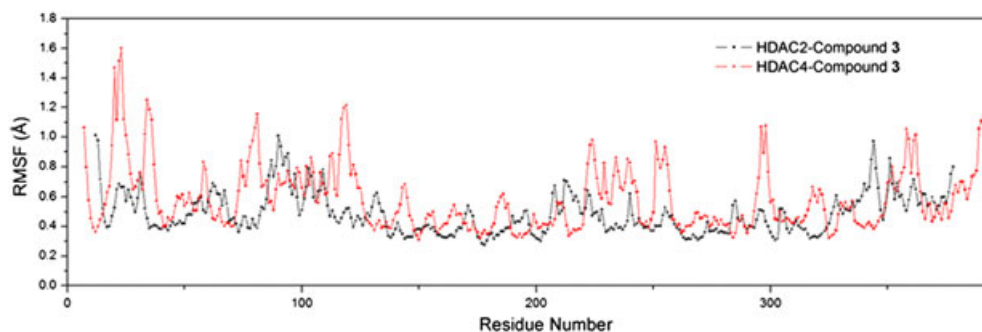
Figure 10. RMSF for all residues during the last 500 ps in MD simulations.
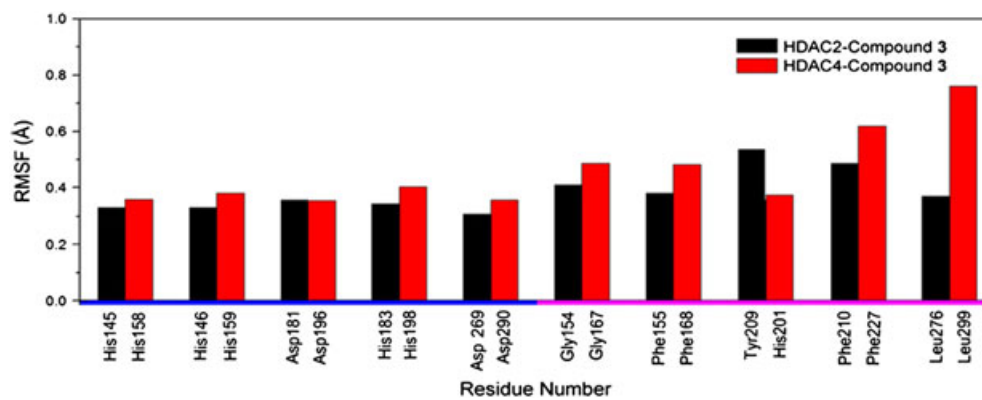
Figure 11. RMSF for residues in the active site during the last 500 ps in MD simulations.
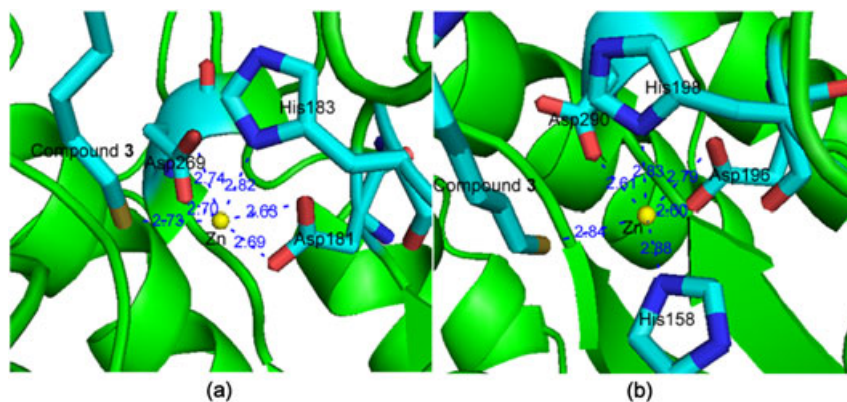
Figure 12. Average zinc ion coordination distances for (a) HDAC2–compound **3** and (b) HDAC4–compound **3** complexes.

Table 3. Hydrogen bonds between compound **3** and HDACs in MD simulations

Enzyme	Donor	AcceptorH	Acceptor	Occupied (%)	Distance (Å)
HDAC2	Compound **3**:S	Tyr308:HH	Tyr308:OH	100.00	2.89
HDAC4	Compound **3**:O_2	His198:HE2	His198:NE2	44.57	3.08
	Compound **3**:O_3	Phe227:H	Phe227:N	42.86	3.22

3 complexes were the same, the sulfur atom of compound **3** occupied one coordination site, and this may be the precondition for the inhibitory activities of these sulfur-containing cyclic tetrapeptide HDACIs.

Hydrogen bonding between ligand and protein play an essential role in stabilizing the complex. The hydrogen bonds formed between compound **3** and HDACs in the active pocket were investigated. As shown in Table 3, the sulfur atom of compound **3** was strongly hydrogen bonded to Tyr308 of HDAC2. The corresponding amino acid residue of Tyr308 is a proline in HDAC4, and there was no hydrogen bond established between the sulfur atom of compound **3** and HDAC4, but the O_2 and O_3 atoms in surface recognition domain of compound **3** formed two weaker hydrogen bond to NE2 atom of His198 and N atom of Phe227, respectively. The hydrogen bonds may be crucial for stabilizing the complexes, and this may be the reason for the similar inhibitory activities to class I and II HDACs of these cyclic tetrapeptides. (The IC_{50} values of compound **1** were 3.9 nM against HDAC1 and 1.8 nM against HDAC4, respectively [38].)

Conclusions

We have successfully synthesized several sulfur-containing cyclic tetrapeptides that can act as HDACIs, and all of them showed potent HDAC inhibitory and anticancer activities. The slight change of the surface recognition domain of these inhibitors by introduction of methyl groups on the aromatic ring of the L-Phe residue within the peptide appeared to have no obvious change in their HDAC inhibitory and anticancer activities. The molecular modeling studies gave us the information about how this series of HDACIs interacted with class I and II HDACs, and it showed that all compounds bind to HDACs were almost in the same mode. The interaction mechanisms of HDAC2 and HDAC4 with these inhibitors were similar but had some differences. Coordinating the zinc ion in the active site of HDACs by the sulfur atom of these inhibitors was the precondition for their inhibitory activities. Both the surface recognition and metal binding domains of these inhibitors could form hydrogen bond with HDACs, so exhibiting similar affinity for class I and II HDACs. The hydrophobic interactions between HDACs and these cyclic tetrapeptides were also very important for stabilizing the enzyme–inhibitor complexes. The data generated from this study would allow us to design some novel cyclic tetrapeptides with different surface recognition and metal binding domains that may act as potent HDACIs.

References

1 Verdin E, Histone Deacetylases-Transcriptional Regulation and other Cellular Functions. Humana Press Inc.: Totowa, NJ, 2006.
2 Drummond DC, Noble GK, Kirpotin DB, Guo Z, Scott GK, Benz CC. Clinical development of histone deacetylase inhibitors as anticancer agents. *Annu. Rev. Pharmacol. Toxicol.* 2005; **45**: 495–528.
3 De Ruijter AJ, van Gennip AH, Caron HN, Kemp S, van Kuilenburg AB. Histone deacetylases (HDACs): characterization of the classical HDAC family. *Biochem. J.* 2003; **370**: 737–749.
4 Voelter-Mahlknecht S, Ho AD, Mahlknecht U. Chromosomal organization and localization of the novel class IV human histone deacetylase 11 gene. *Int. J. Mol. Med.* 2005; **16**: 589–598.
5 Michan S, Sinclair D. Sirtuins in mammals: insights into their biological function. *Biochem. J.* 2007; **404**: 1–13.
6 Bressi JC, Jennings AJ, Skene R, Wu YQ, Melkus R, Jong RD, Shawn O, Grimshaw CE, Navre M, Gangloff AR. Exploration of the HDAC2 foot pocket: synthesis and SAR of substituted *N*-(2-aminophenyl)benzamides. *Bioorg. Med. Chem. Lett.* 2010; **20**: 3142–3245.
7 Bottomley M, Lo SP, Di Giovine P, Cirillo A, Scarpelli R, Ferrigno F, Jones P, Neddermann P, De Francesco R, Steinkuhler C, Gallinari P, Carfi A. Structural and functional analysis of the human HDAC4 catalytic domain reveals a regulatory zinc-binding domain. *J. Biol. Chem.* 2008; **283**: 26694–26704.
8 Somoza JR, Skene RJ, Katz BA, Mol C, Ho JD, Jennings AJ, Luong C, Arvai A, Buggy JJ, Chi E, Tang J, Sang BC, Verner E, Wynands R, Leahy EM, Dougan DR, Snell G, Navre M, Knuth MW, Swanson RV, McRee DE, Tari LW. Structural snapshots of human HDAC8 provide insights into the class I histone deacetylases. *Structure* 2004; **12**: 1325–1334.
9 Johnstone RW. Histone-deacetylase inhibitors: novel drugs for the treatment of cancer. *Nat. Rev. Drug Discov.* 2002; **1**: 287–299.
10 Marks PA, Dokmanovic M. Histone deacetylase inhibitors: discovery and development as anticancer agents. *Expert Opin. Investig. Drugs* 2005; **14**: 1497–1511.
11 Yoshida M, Kijima M, Akita M, Beppu T. Potent and specific inhibition of mammalian histone deacetylase both in vivo and in vitro by trichostatin A. *J. Biol. Chem.* 1990; **265**: 17174–17179.
12 Richon VM, Emiliani S, Verdin E, Webb Y, Breslow R, Rifkind RA, Marks PA. A class of hybrid polar inducers of transformed cell differentiation inhibits histone deacetylases. *Proc. Natl. Acad. Sci. U.S.A.* 1998; **95**: 3003–3007.
13 Singh SB, Zink DL, Polishook JD, Dombrowski AW, Darkin-Rattray SJ, Schmatz DM, Goetz MA. Apicidins: novel cyclic tetrapeptides as coccidiostats and antimalarial agents from *Fusarium pallidoroseum*. *Tetrahedron Lett.* 1996; **37**: 8077–8080.
14 Ueda H, Nakajima H, Hori Y, Fujita T, Nishimura M, Goto T, Okuhara M. Action of FR901228, a novel antitumor bicyclic depsipeptide produced by *Chromobacterium violaceum* no. 968, on Ha-ras transformed NIH3T3 cells. *J. Antibiot.* 1994; **47**: 301–310.
15 Ueda H, Manda T, Matsumoto S, Mukumoto S, Nishigaki F, Kawamura I, Shimomura K. FR901228, a novel antitumor bicyclic depsipeptide produced by *Chromobacterium violaceum* no. 968. Ill. Antitumor activities on experimental tumors in mice. *J. Antibiot.* 1994; **47**: 315–323.
16 Furumai R, Matsuyama A, Kobashi N, Lee KH, Nishiyama M, Nakajima H, Tanaka A, Komatsu Y, Nishino N, Yoshida M, Horinouchi S. FK228 (depsipeptide) as a natural prodrug that inhibits class I histone deacetylases. *Cancer Res.* 2002; **62**: 4916–4921.
17 Closse A, Hugenin R. Isolation and structural clarification of chlamydocin. *Helv. Chim. Acta* 1974; **57**: 533–545.
18 De Shepper S, Bruwiere H, Steller U, Andries L, Wouters W, Janicot M, Arts J, Van Heusden J. Inhibition of histone deacetylases by chlamydocin induces apoptosis and proteasome-mediated degradation of survivin. *J. Pharmacol. Exp. Ther.* 2003; **304**: 881–888.

19 Gururaj MS, Satoshi A, Tamaki K, Norikazu N, Satoko M, Tomonori GN and Minoru Y. Molecular design of histone deacetylase inhibitors by aromatic ring shifting in chlamydocin framework. *Bioorgan. Med. Chem.* 2007; **15**: 7830–7839.

20 Rodriquez M, Terracciano S, Cini E, Settembrini G, Bruno I, Bifulco G, Taddei M, Gomez-Paloma L. Total synthesis, NMR solution structure, and binding model of the potent histone deacetylase inhibitor FR235222. *Angew. Chem. Int. Ed.* 2006; **118**: 437–441.

21 Maulucci N, Chini MG, Micco SD, Izzo I, Cafaro E, Russo A, Gallinari P, Paolini C, Nardi MC, Casapullo A, Riccio R, Bifulco G, Riccardis FD. Molecular insights into azumamide E histone deacetylases inhibitory activity. *J. Am. Chem. Soc.* 2007; **129**: 3007–3012.

22 Li XH, Wang G, Li JX, Xiu ZL, Nishino N. Synthesis and resolution of Boc-L-methylphenylalanines. *Chem. J. Chinese U.* 2008; **29**: 1363–1366.

23 Huey R, Morris GM, Olson AJ, Goodsell DS. A semiempirical free energy force field with charge-based desolvation. *J. Comput. Chem.* 2007; **28**: 1145–1152.

24 Morris GM, Goodsell DS, Halliday RS, Huey R, Hart WE, Belew RK, Olson AJ. Automated docking using a Lamarckian genetic algorithm and an empirical binding free energy function. *J. Comput. Chem.* 1998; **19**: 1639–1662.

25 Wang DF, Helquist P, Wiech NL, Wiest O. Toward selective histone deacetylase inhibitor design: homology modeling, docking studies, and molecular dynamics simulations of human class I histone deacetylases. *J. Med. Chem.* 2005; **48**: 6936–6947.

26 Wallace AC, Laskowski RA, Thornton JM. LIGPLOT: a program to generate schematic diagrams of protein-ligand interactions. *Protein Eng.* 1995; **8**: 127–134.

27 Case DA, Darden TA, Cheatham TE, Simmerling CL, Wang J, Duke RE, Luo R, Merz KM, Pearlman DA, Crowley M, Walker RC, Zhang W, Wang B, Hayik S, Roitberg A, Seabra G, Wong KF, Paesani F, Wu X, Brozell S, Tsui V, Gohlke H, Yang L, Tan C, Mongan J, Hornak V, Cui G, Beroza P, Mathews DH, Schafmeister C, Ross WS, Kollman PA. AMBER version 9, University of California: San Francisco, CA, 2006.

28 Wang JM, Cieplak P, Kollman PA. How well does a restrained electrostatic potential (RESP) model perform in calculating conformational energies of organic and biological molecules? *J. Comput. Chem.* 2000; **21**: 1049–1074.

29 Wang J, Wolf RM, Caldwell JW, Kollamn PA, Case DA. Development and testing of a general amber force field. *J. Comput. Chem.* 2004; **25**: 1157–1174.

30 Jakalian A, Bush BL, Jack DB, Bayly CI. Fast, efficient generation of high-quality atomic charges. AM1-BCC model: I. Method. *J. Comput. Chem.* 2000; **21**: 132–146.

31 Stote RH, Karplus M. Zinc binding in proteins and solution: a simple but accurate nonbonded representation. *Proteins* 1995; **23**: 12–31.

32 Wang JM, Wang W, Kollman PA. ANTECHAMBER: an accessory software package for molecular mechanical calculations. *Abstr. Pap. Am. Chem. Soc.* 2001; **222**: 403.

33 Jorgensen WL, Chandrasekhar J, Madura JD, Impey RW, Klein ML. Comparison of simple potential functions for simulating liquid water. *J. Chem. Phys.* 1983; **79**: 926–935.

34 Darden T, York D, Pedersen L. Particle mesh Ewald-an N.Log(N) method for Ewald sums in large systems. *J. Chem. Phys.* 1993; **98**: 10089–10092.

35 Ryckaert JP, Ciccotti G, Berendsen HJC. Numerical integration of the Cartesian equations of motion of a system with constraints: molecular dynamics of *n*-alkanes. *J. Comput. Phys.* 1977; **23**: 327–341.

36 Berendsen HJC, Postma JPM, Vangunsteren WF, Dinola A, Haak JR. Molecular dynamics with coupling to an external bath. *J.Chem. Phys.* 1984; **81**: 3684–3690.

37 Honig B, Nicholls A. Classical electrostatics in biology and chemistry. *Science* 1995; **268**: 1144–1149.

38 Hirashima Y, Kato T, Nishino N, Maeda S, Nishino TG, Yoshida M. Design and synthesis of histone deacetylase inhibitors by aromatic ring shifting in chlamydocin framework. In Proceedings of 29th European Peptide Symposium (Peptides), 2006; 758–759.